E-144 internal note

Cross-calibration of E-144 Cherenkov monitors with the electron calorimeter

Glenn Horton-Smith

February 9, 1998

Abstract

Previously-obtained calibration constants for the N2MO and N3MO detectors led to inconsistencies between our model predictions and the reported number of electrons observed by the detectors in the data from August 1996, the first run for which the detectors were available. This disagreement led us to distrust the calibration constants as given by Field[1], and to rescale those constants by large factors (about eight) when estimating the laser intensity with "constrained fits" of the Cherenkov monitor data[2]. In this note, a cross-calibration of N2MO and N3MO with the electron calorimeter is presented. The cross-calibration gives results within a factor of three of the original, unscaled calibration. It is further shown that no large scale factors are required with the new calibration.

1 Introduction

Previously-obtained calibration constants led to inconsistencies between our model predictions and the reported number of electrons observed by the Cherenkov detectors N2MO, N3MO, EC31, and EC37 in the data from August 1996, the first run for which the detectors N2MO and N3MO were available. This disagreement led us to rescale the calibration constants by large factors: roughly a factor of 8 for both N2MO and N3MO, and a factor of 1.6 for "linear" electron counters.[2]

Our justification for this rescaling was that the ECAL data from March 1995, after "reconstruction" and normalization by the total number of backscattered photons, showed substantial agreement with the model, to within experimental uncertainties. The experimental uncertainties in the March data were roughly $\pm15\%$ in η and $\pm10\%$ in the reconstructed ECAL signal, leading to an overall $\pm30\%$ uncertainty in the normalized $n = 2$ data and $\pm60\%$ (i.e., a factor of 2) in the normalized $n = 3$ data. The rescaling required for N2MO and N3MO to obtain consistency in the August 1996 data was substantially greater than the experimental uncertainty in the March 1995 confirmation of the nonlinear Compton scattering theory, and so it was concluded that the cause of the discrepancy must lie in the calibration of the detectors. However, the large rescaling factor was not understood, and all of us found that disturbing.

It should be noted that the March 1995 results were obtained with experimental parameters somewhat different than in August 1996. All data in August 1996 was taken with the green, linearly-polarized laser, at η ranging from 0.2 to 0.4 (according to the Cherenkov monitor fits). N2MO intercepted electrons from 12.3 to 13.1 GeV/c. Our best data confirming the correctness of the accepted theory in modeling the flux of electrons scattered off the green laser into this momentum range comes from approximately 5000 events taken with green, *circularly*-polarized laser at η from 0.02 to 0.2. (Due to manpower limitations, the data taken with linearly-polarized green laser in March 1995 has not been as carefully studied as the circular.) We analyze N2MO based on theory not tested by experiment. This is not necessarily an improper thing to do, since we are still testing the overall internal consistency of the theory, but it is a point to be borne in mind.

It should also be remembered that the agreement between simulation and experiment is not particularly good in the March 1995 data, as discussed in a note presented at our September 9, 1996 meeting[3]. A χ^2/(degree of freedom) of 141/44 was calculated for the green-circular data which we still intend to present in the Phys. Rev. D paper.

Finally, an arbitrary shift of the Cherenkov monitor calibration rescaling factors can result in different predictions for η with equally good internal consistency of the constrained fits. For example, rescaling the "linear", N2MO, and N3MO counters by 1.6, 4.0, and 2.0, respectively, instead of 1.6, 8.0, and 8.0, would also give internally consistent readings but increase the intensity estimate by a factor of two.

All of these considerations and uncertainties motivated a second-look at the Cherenkov monitor calibration, this time using actual data taken in August 1996 to cross-calibrate N2MO and N3MO with ECAL, whose calibration is not in question.

2 Cross-calibration of N2MO and N3MO with ECAL

Below, the measurements of the acceptance functions of N2MO and N3MO are reviewed; a cross-calibration of N2MO, N3MO, and ECAL using a bremsstrahlung spectrum from wire scans and PCAL "wire data" runs is presented; a direct cross-calibration of N3MO with ECAL using green laser data is presented; and the effect of different assumed acceptance functions is analyzed.

2.1 The acceptance of N2MO and N3MO

The primary purpose of the Cherenkov monitors is to tell us the scattering rate of electrons into a relatively narrow range of momentum near some central momentum, *i.e.*, dN_{e-}/dp near 12.7 GeV/c for N2MO and near 8.9 GeV/c for N3MO. For this reason, the monitors were designed with narrow acceptances and placed in the flattest portions of the electron spectrum.

The "as-built" acceptances of the monitors were measured using test-beam momentum scan data. Figures 1 and 2 show the data from these runs. [Runs 15017 and 15026 for N2MO and 15009 for N3MO.] The horizontal axis is test beam momentum as communicated to the E-144 DAQ through the "SAM" (Smart Analog Monitor) channel, and the vertical axis is ADC counts per incident electron as measured by the ECAL. The data is fitted to the sum of two square apertures "smeared" by the test-beam momentum spread and vertical size. The fitted acceptance with test-beam size set to zero is also shown.

The "standard" E-144 analysis used a single square aperture with different edges. Figures 3 and 4 show the best fit to the data obtained by varying normalization and smearing parameter while maintaining the edges at the "standard" acceptances. These parameters are specified in the `n2n3_par.lut` file used for the last round of n-tuple generation.

The parameters of the fit are identified in Table 1. The results of the two-box fit are given in Table 2, and the "standard" acceptance parameters are given in Table 3.

As noted previously, the precision of the calibration in terms of number of electrons in some unremarkable acceptance is less relevant than the accuracy of the estimate of dN_{e-}/dp provided. The dN_{e-}/dp result should be more-or-less unchanged by re-analysis of the acceptance. Likewise, such re-analysis should produce an equal scaling of the constant for converting ADC counts to observed electron count and of the range over which the simulated spectrum is integrated to calculate the simulated electron count. Therefore, in the following subsections, calibration constants will be given in units of electrons per GeV/c per ADC count, rather than total electrons per ADC count. Once a specific acceptance is chosen, the former type of calibration constant can easily be converted to the latter. The effect of different acceptance functions on the analysis will be discussed in a later subsection.

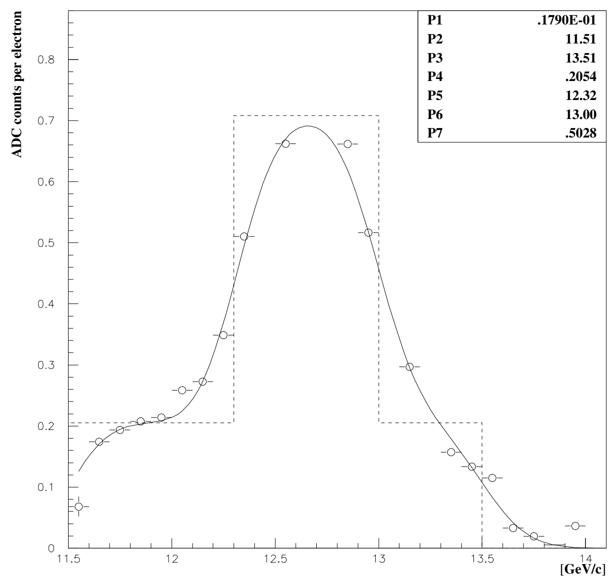

Figure 1: Acceptance of N2MO. Data points come from test beam momentum scans. Dashed line shows the two-box acceptance function, solid line the fit assuming a Gaussian shape to the test beam. The parameters of the fit are identified in Table 1.

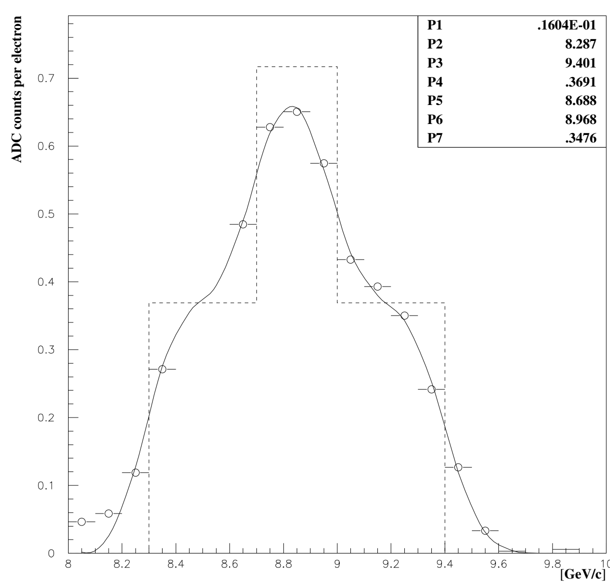

Figure 2: Acceptance of N3MO. Data points come from test beam momentum scans. Dashed line shows the two-box acceptance function, solid line the fit assuming a Gaussian shape to the test beam. The parameters of the fit are identified in Table 1.

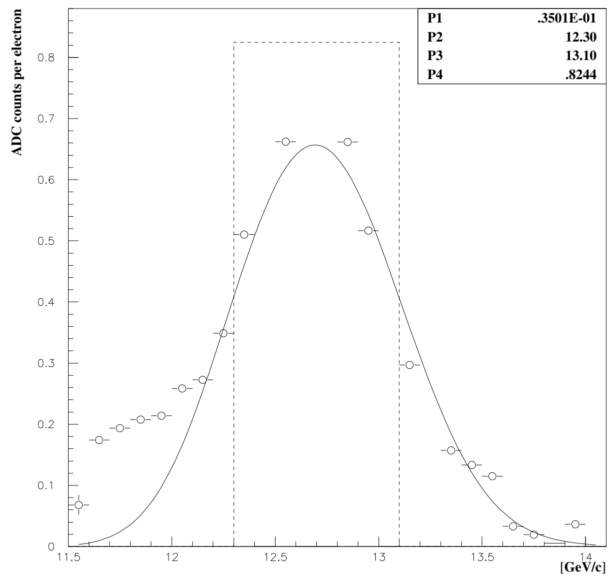

Figure 3: Same data as in Fig. 1, with the square acceptance used for the most recent round of n-tuple generation. The normalization for this figure was chosen by fitting for minimum chi-squared.

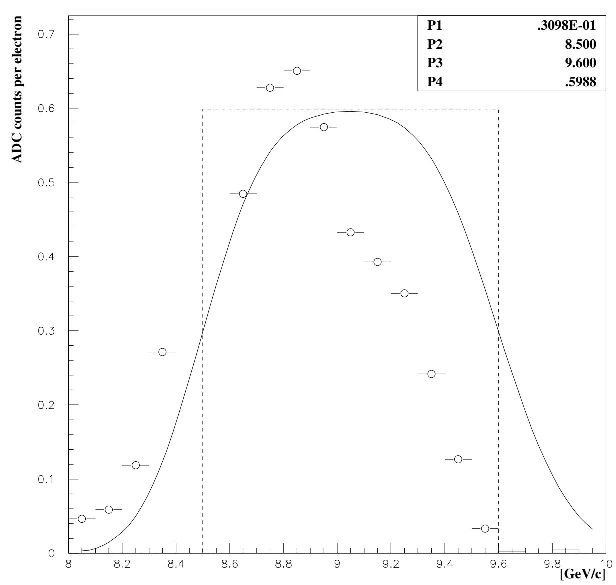

Figure 4: Same data as in Fig. 2, with the square acceptance used for the most recent round of n-tuple generation. The normalization was chosen by fitting for minimum chi-squared, with normalization chosen by fitting with upper edge at 9.3 GeV/c. (See footnotes to Table 3.)

parameter number	parameter description	units
1	fractional momentum spread (rms/mean)	-
2	low edge, box 1	GeV/c
3	high edge, box 1	GeV/c
4	constant, box 1	ADC counts per electron
5	low edge, box 2	GeV/c
6	high edge, box 2	GeV/c
7	constant, box 2	ADC counts per electron

Table 1: Description of the parameters of the fits in Figs. 1 through 4. Parameters 5-7 do not appear in the single-box fits.

detector	low edge 1 [GeV/c]	high edge 1 [GeV/c]	const. 1 [ADC/e-]	low edge 2 [GeV/c]	high edge 2 [GeV/c]	const. 2 [ADC/e-]	mean mom. [GeV/c]	eff. width [GeV/c]
N2MO	11.5	13.5	0.21	12.3	13.0	0.50	12.6	1.1
N3MO	8.30	9.40	0.37	8.70	9.00	0.35	8.85	0.70

Table 2: Values of the fitted parameters for the two-box fits to the test-beam acceptance scan data. The "mean momentum" is the mean value of the momentum p weighted by the acceptance function. The "effective width" is the total area under the acceptance function divided by the peak value of the (unsmeared) acceptance function. The constants are from the fits to the test beam data; they are not the calibration constant for the August 1996 data as such, although similar data was combined with other knowledge to obtain the original calibration constants[1].

detector	low edge [GeV/c]	high edge [GeV/c]	mean momentum [GeV/c]	width [GeV/c]
N2MO	12.3	13.1	12.7	0.8
N3MO	8.50	9.60[1]	9.05[2]	1.10[3]

[a] N.B. Some early versions of the `n2n3_par.lut` file have 9.3 GeV/c for the high edge of N3MO's acceptance, which would give a better match to the data and also give a width closer to the two-box "effective width." The parameter that was used for the last n-tuple generation is 9.6 GeV/c as quoted. The effect of different acceptances is discussed in a later subsection.

[b] Central momentum is 8.80 GeV/c if high edge is 9.3 GeV/c.

[c] Width is 0.8 GeV/c if high edge is 9.3 GeV/c.

Table 3: Values of the standard parameters for the single box acceptance of N2MO and N3MO.

detector	inferred flux [e-/(GeV/c)]	average reading [ADC counts]	calibration constant [e-/(GeV/c)/count]
N2MO, Aug. 3	204 ± 4	$12.4 \pm .7$	16.5 ± 1.0
N3MO, Aug. 3	187 ± 4	257 ± 12	$0.73 \pm .04$
N2MO, Aug. 8	325 ± 1	$11.8 \pm .1$	27.5 ± 0.3
N3MO, Aug. 8	298 ± 1	219 ± 2	$1.36 \pm .01$

Table 4: Results of the indirect calibration of N2MO and N3MO with ECAL using bremsstrahlung. The quoted errors represent statistical errors only.

2.2 The indirect cross-calibration of N2MO and N3MO with ECAL using bremsstrahlung

In the midst of taking laser-collision data, time was taken for acquisition of "wire" data for calibration of the PCAL energy-vs-position map. This data also provides a known spectrum for calibrating the N2MO and N3MO detectors, with only one degree of freedom: the total flux of electrons in the data sample. This single unknown is well measured by the ECAL.

The runs used in this analysis are wire scans 15140 and 15142, taken August 3, 1996, and PCAL calibration data runs 15530 through 15537, taken August 8, 1996. The ECAL position in the latter set of runs was -120 mm, so the top of the top row was at -245 mm in E144's "PCS" coordinate system. According to the spectrometer map, the top row intercepted electrons from 7.62 to 8.49 GeV/c, so it did not quite overlap the core of the N3MO acceptance. Because no ECAL row was directly behind the counters we wish to cross-calibrate, we have no direct measurement of the number of electrons passing through the counters in these runs. However, the average flux can be inferred and compared to the average ADC reading. In wire scans 15140 and 15142, the ECAL was behind N3MO but still below N2MO.

In this analysis, the top four rows of the ECAL are used to measure the total rate. Beam charge data from the Beam Containment System toroids was not available for these runs, so the fifth row of ECAL is used as a somewhat-independent quality cut to eliminate beam pulses with low rate. The total energy deposited in each row is divided by the mean energy of individual electrons accepted by that row and the width of the momentum acceptance for the row to obtain an estimate of the differential scattering rate at each momentum. This data is plotted in Figs. 5 and 7 (for the August 8 and August 3 data, respectively) and fitted to a bremsstrahlung spectrum. The fitted bremsstrahlung spectrum is extrapolated to the central momenta of the two counters, N2MO and N3MO. From this data, the average number of electrons per GeV/c is known for each detector for this data set.

Using the same events from the same data set, the pedestal-subtracted ADC readings from the two counters are plotted in Fig. 6 and 8. (Pedestals were measured using events for which the ECAL read little or no deposited energy.) From this data, the average ADC reading of each detector is known for the corresponding average number of electrons per GeV/c measured with the ECAL data. Dividing one by the other gives the calibration in terms of electrons per GeV/c per ADC count. This data is summarized in Table 4.

There is a factor of two discrepancy between the two calibrations. This cannot be due to the position of the calorimeter, as the effect of ECAL position on N3MO operation, if any, is very small, as shown in Fig. 9, and the vacuum chamber window extends below 6.0 GeV/c. The difference in calibration constants could represent a real change in N3MO calibration between August 3 and August 8. It could also be an effect of the unusual steering in place on August 8, although the horizontal "bump" of 1 mm should have been negligible for these detectors.

It will be noted that N2MO reads very low in these conditions, a result of it being configured for its normal mode of operation where it sees an order of magnitude more flux than N3MO. Extrapolating

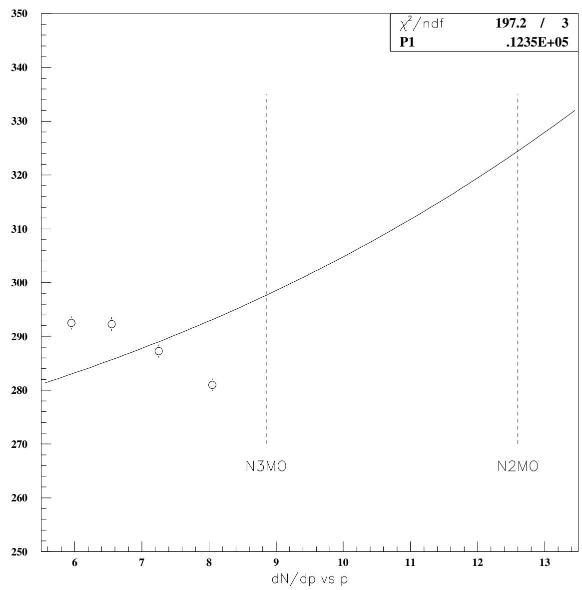

Figure 5: Bremsstrahlung spectrum as measured by the ECAL, from PCAL wire data taken August 8, 1996. Each data point represents one row of ECAL: the horizontal axis is the row central momentum, and the vertical axis gives number of electrons per GeV/c in the row's momentum acceptance. The error bars on the points give the root-mean-square of the data divided by the square root of the number of events. The solid curve is a bremsstrahlung spectrum with best-fit normalization. Central momenta of N2MO and N3MO are indicated with dashed lines. The deviation of the data points from the fit exceeds the statistical spread of the data. These residuals are all less than 6% of the signal and may be due to systematic effects in ECAL reconstruction or calibration.

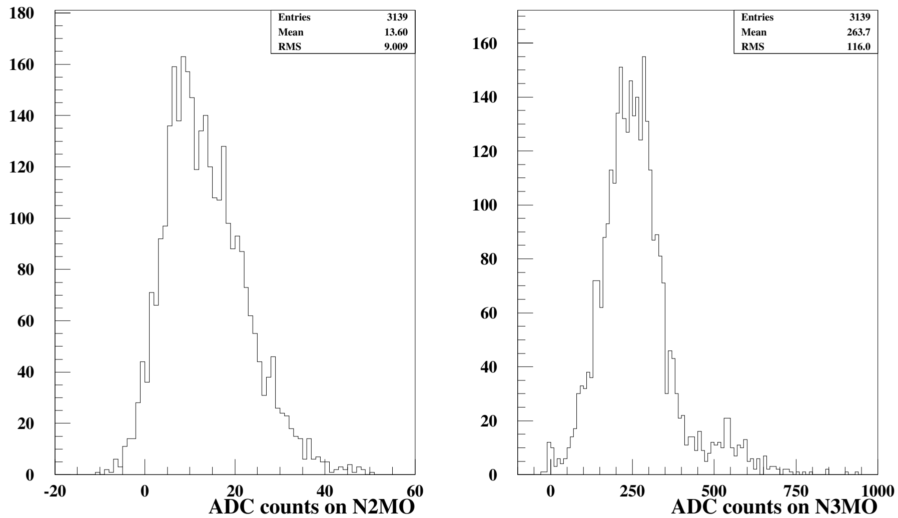

Figure 6: Frequency distribution of ADC readings, after pedestal correction, for runs 15530-15537 (August 8, 1996 data). N2MO is on the left, N3MO on the right.

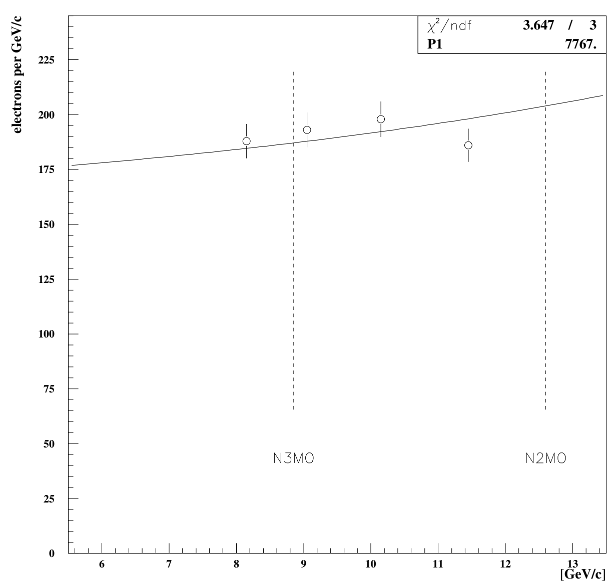

Figure 7: Bremsstrahlung spectrum as measured by the ECAL for wire scans 15140 and 15142 (August 3, 1996).

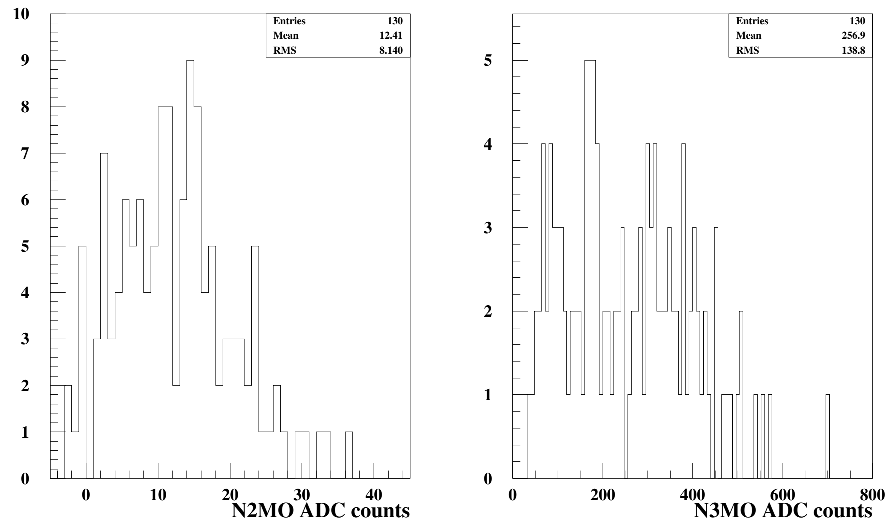

Figure 8: Frequency distribution of ADC readings for wire scans 15140 and 15142.

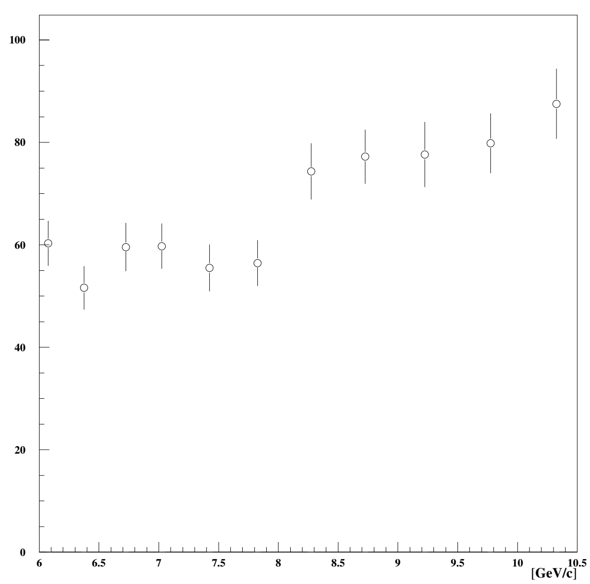

Figure 9: N3MO ADC normalized by linear detector, plotted versus central momentum of the top ECAL row, for ECAL scan 15296. A slight (less than 10%) shift in average reading may occur as the top of the ECAL passes behind N3MO, but this could also be a coincidental change in collision conditions.

from low ADC counts should not be too much of a problem, however, since N2MO and N3MO were read out with a LeCroy 2249 ADC, which is much more linear at its low end than the Phillips QDC used for the $n = 1$ rate monitors. The residuals on the ECAL fit suggest systematic uncertainties of at least $\pm 6\%$ may be present.

As a further aid to visualizing the cross-calibration data, two-dimensional density plots of N2MO and N3MO readings versus the top row of ECAL are shown in Fig. 10, with lines drawn representing the major axis expected from the calibration constants given above. The scatter in the data arises from the statistics of the electron to photo-multiplier-tube photo-electron conversion and the fact that the top row intercepts different electrons than the detectors, but it can be clearly seen that the cross-calibration is correct.

The calibration constants found above will be compared with the "original" calibration in a later section.

2.3 The direct cross-calibration of N3MO with ECAL using nonlinear Compton data

A direct cross-calibration can be done with any run for which part of the ECAL was directly behind the monitor of interest. Unfortunately, there is no data for which the ECAL was directly behind N2MO. (The ECAL mover would have to have been set to above -60 mm, and the highest position recorded was -70 mm.) However, there is plenty of data to provide a direct N3MO calibration.

The analysis below uses data from ECAL scan 15296, which is an actual, positron-producing run (arguably our first and best), with N2MO and N3MO in their final data-taking configurations. This data was taken on August 5, 1996. Events were required to have at least 10^6 forward photons as detected by EC31/EC37. The spectrum varies nearly linearly with momentum in the range of interest, both in theory (Fig. 11) and in observation (Fig. 12). The number of electrons per GeV/c averaged over the acceptance of the counter is therefore the same as the number of electrons per GeV/c at the center of the counter's acceptance, which can be determined by interpolating between the two nearest calorimeter rows.

Figure 13 shows the N3MO ADC plotted versus the ECAL estimate of $dN_{e-,\mathtt{N3MO}}/dp$, for events when at least one row of ECAL was above and one below the N3MO central momentum of 8.85 GeV/c. The inverse of the slope is $0.65 \pm .01$ electrons per GeV/c per ADC count, where the error comes from the fit covariance matrix. Significant scatter of the data is evident. Figure 14 shows the electron yield in the ECAL in the $n = 3$ region normalized by the N3MO ADC. The intercept of the fitted line with 8.85 GeV/c is at $0.62 \pm .01$ GeV/c per ADC count, where again the error quoted is from the canonical fit error estimate. Folding in likely ECAL reconstruction systematic errors, the cross-calibration using laser-scattered electrons with ECAL directly behind N3MO gives a calibration constant of 0.63 ± 0.01 stat. $\pm$ .04 syst., which is consistent with the August 3 cross-calibration.

2.4 Effect of different assumed acceptances of N2MO and N3MO

The calibration constants calculated above convert from ADC counts to electron yield per unit momentum at the central momentum of the detector's acceptance. Any systematic errors in this conversion due to the finite width of the momentum acceptance must come from second-order and higher derivatives of the spectrum w.r.t. momentum, and since both the bremsstrahlung and nonlinear Compton spectra are very linear with momentum in the ranges of interest, this error is small. Figures 15 and 16 show the effects of varying momentum acceptances on N2MO and N3MO, based on simulated spectra.

Systematic calibration errors could also come from misidentification of the detector central momentum. Figures 17 and 18 show the fractional error introduced by central momentum misidentification, obtained by shifting the acceptance functions described in Table 2 and applying them to simulated spectra. Again, the possible systematic errors are small.

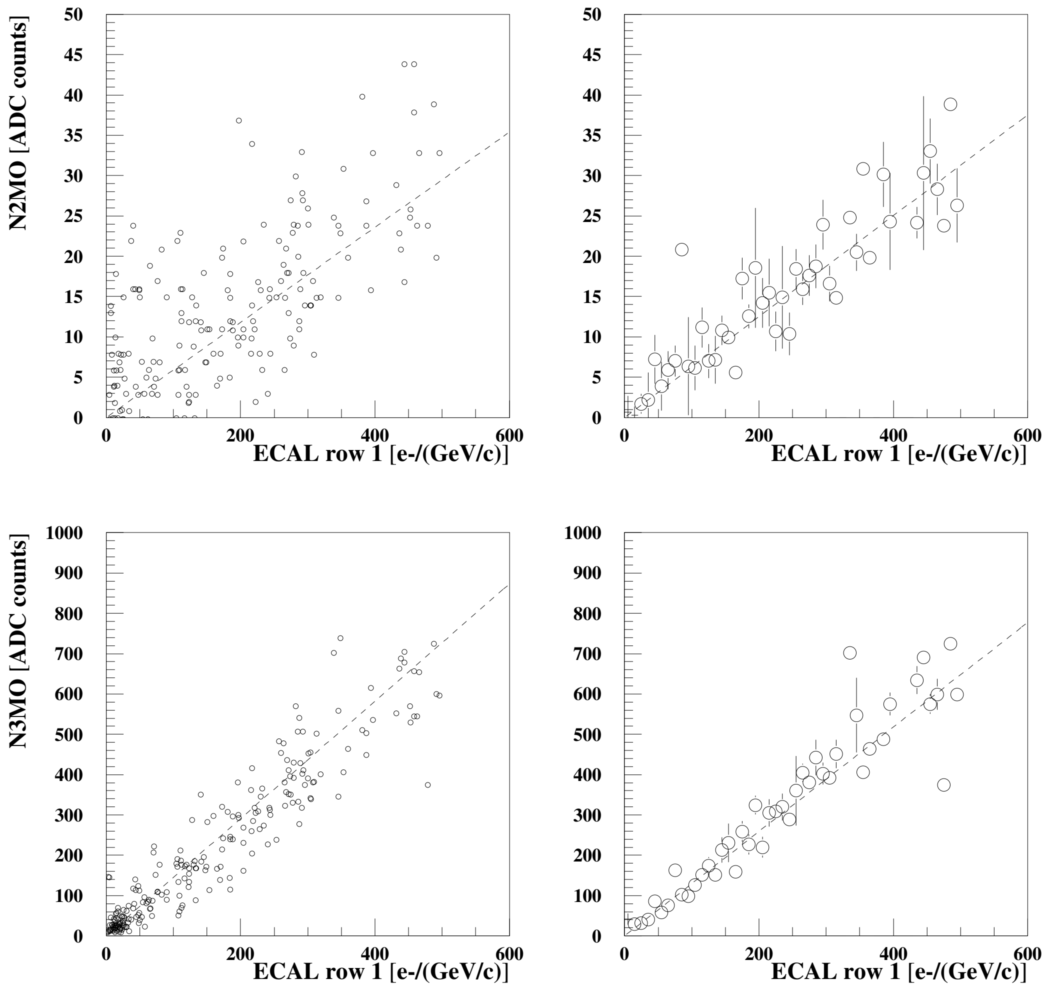

Figure 10: Two-dimensional scatter plots (left) and profile histograms (right) of ADC readings versus energy deposited in the top row of ECAL. The lines are calculated based on the calibration constants in Table 4, the acceptance of the top row, and the shape of the bremsstrahlung spectrum. Data is from the wire scans 15140 and 15142.

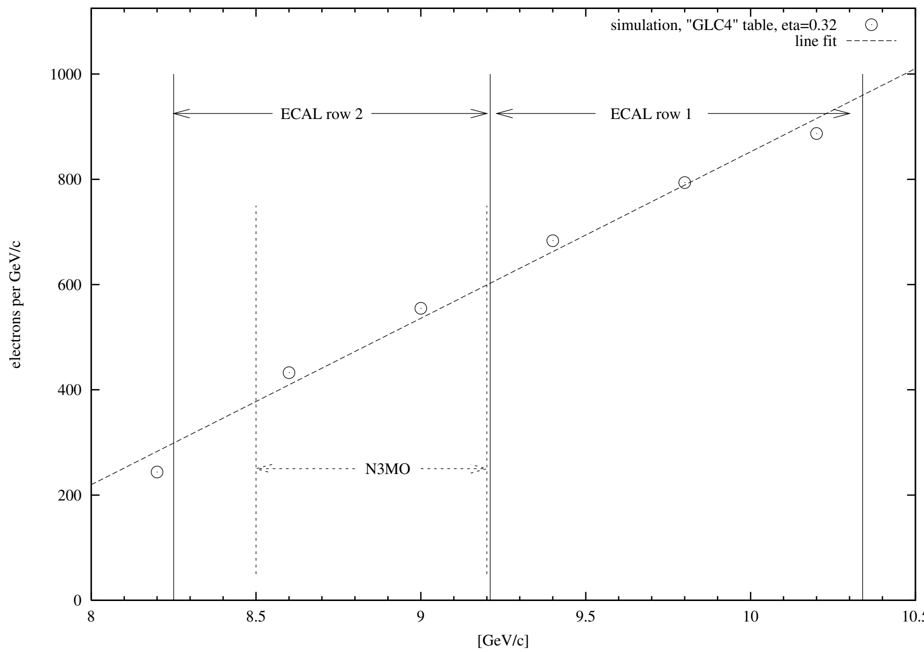

Figure 11: Simulated spectrum for the linear-green laser with edges indicated for N3MO and ECAL at -92 mm (top of top row at -217 mm in "PCS"). Parameters were $\eta = 0.3162$, $A_{\mathrm{eff}} = 29.9\,\mu^2$, $\tau = 1.5$ psec (FWHM), $E_{e-} = 46.6$ GeV, $\sigma_{e-,x} = 25\ \mu$, $\sigma_{e-,y} = 40\ \mu$, $\tau_{e-} = 7$ psec (FWHM).

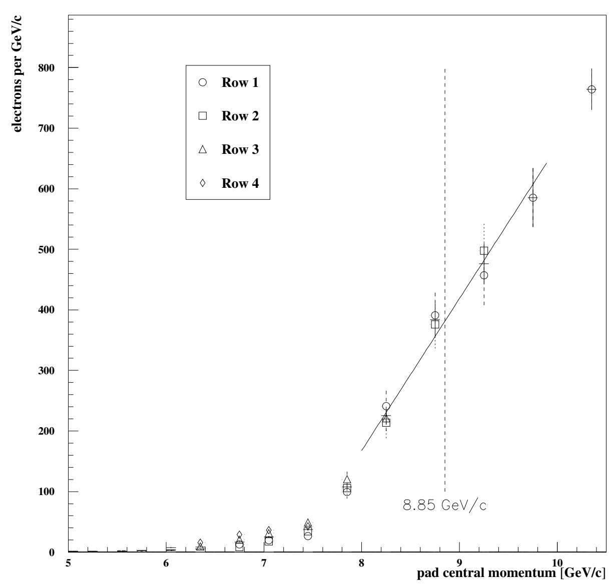

Figure 12: Observed spectrum from run 15296. All reconstructed rows give the same answer in the region of interest.

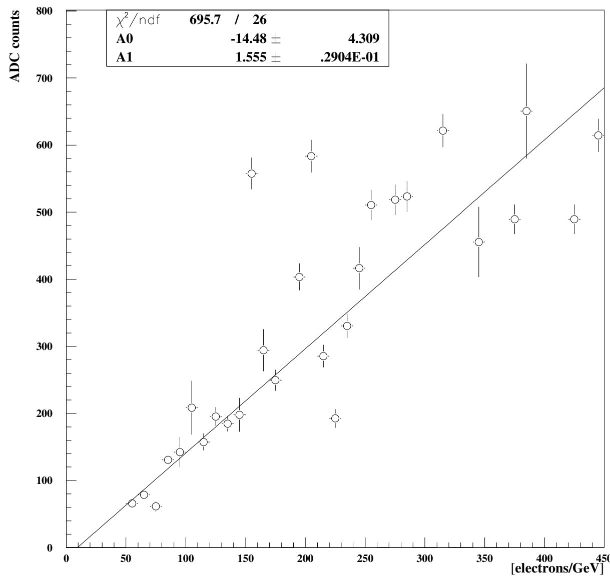

Figure 13: Average N3MO ADC averaged and plotted in bins of ECAL-based estimate of number electrons per GeV/c at 8.85 GeV/c.

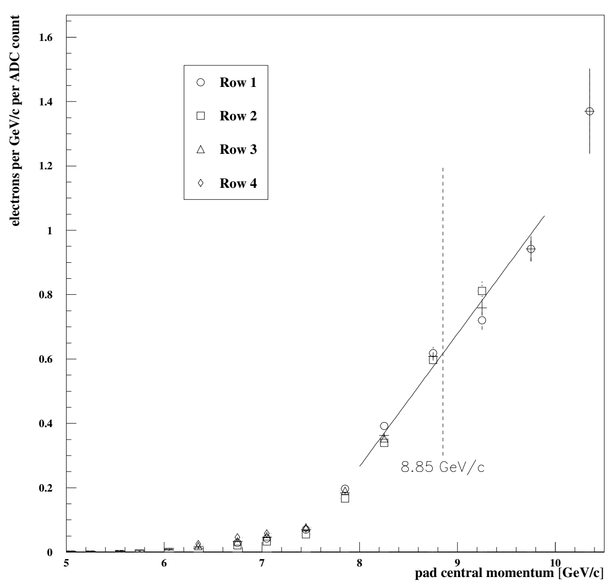

Figure 14: Observed spectrum from run 15296 normalized by N3MO ADC. The intercept of the fitted line with the N3MO central momentum gives the calibration constant.

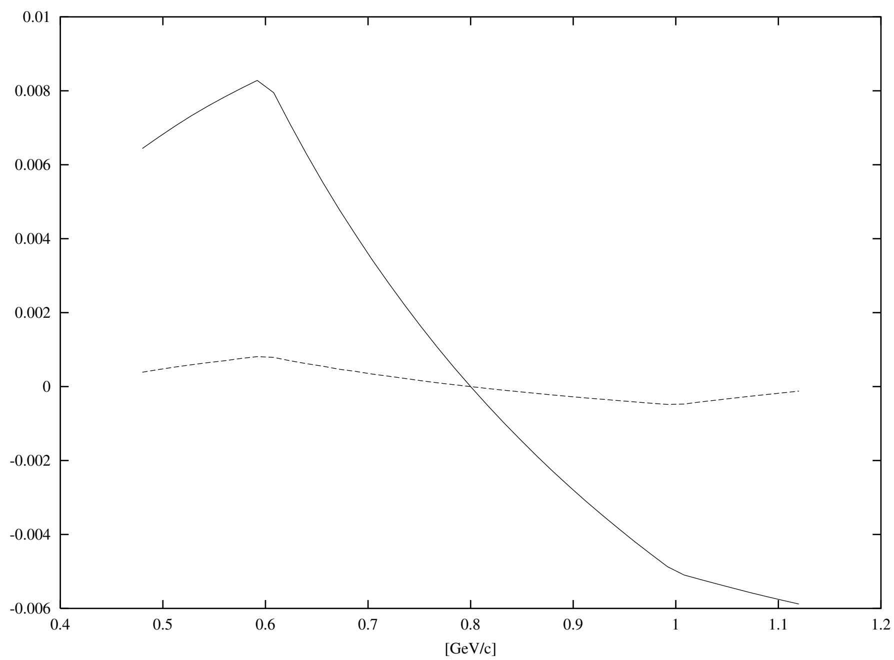

Figure 15: Simulated effect of different acceptance widths on the accuracy of the calibration of N2MO. The horizontal axis is the (effective) width of the acceptance function, and the vertical axis is the fractional deviation of the estimated electron yield from its actual value at the central momentum of the detector, as calculated by the `sum_bin` function from the MSDOS-based E-144 analysis software. The solid line shows the simulation for a nonlinear Compton spectrum and a square aperture of the given width; the dashed line shows the effect with square aperture and a bremsstrahlung spectrum.

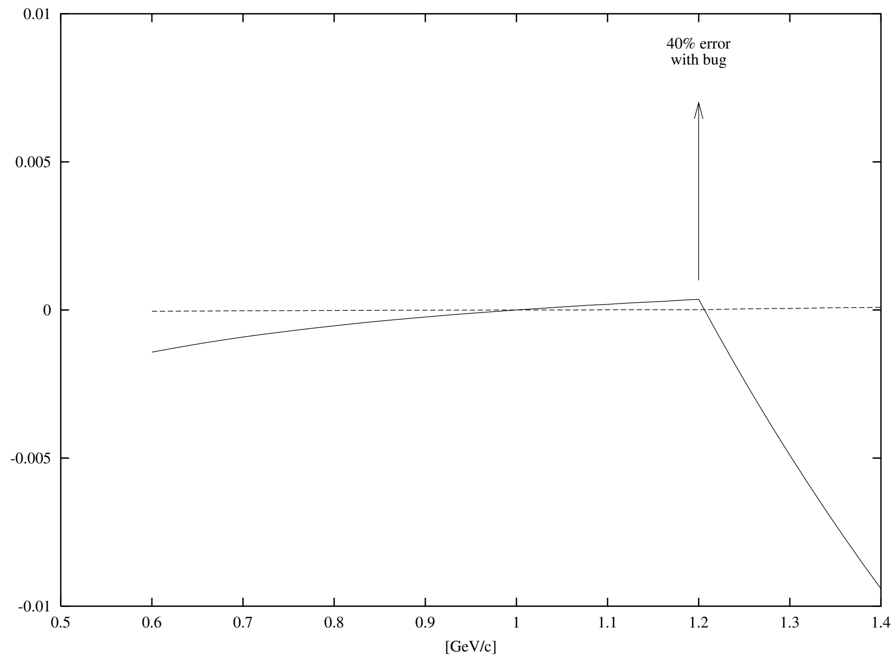

Figure 16: Simulated effect of different acceptance widths on the accuracy of the calibration of N3MO. (See caption for Fig. 15.) A bug in some early versions of the `sum_bin` function caused an extra bin to be added when the upper end of the acceptance fell exactly on a bin edge.

2.5 Calibration of EC31/EC37 with bremsstrahlung

Calibration runs 15460 - 15463, taken August 7, 1996, provide good data for calibrating the linear monitors. This data was taken with an electron beam of 7.1×10^9 e-/pulse incident on the 30-μm-thick aluminum foil at IP1. N2MO readings for this run are consistent with these conditions, assuming the 0.7 e-/(GeV/c)/(ADC count) calibration is correct. (N3MO apparently had its filter removed for this run.) The EC31/10 ADC averaged 3317 counts for this data, and the EC37 ADC averaged 1508 counts. The electron flux from the 46.6-GeV electrons incident on the foil can be calculated as 1.64×10^5 e-/(GeV/c) and 2.92×10^5 e-/(GeV/c) at 31 GeV/c and 37 GeV/c, respectively. The Compton spectrum for the green laser gives values of $dN/dp/N_\gamma$ of 0.0276 e-/photon/(GeV/c) at 31 GeV/c and 0.0320 e-/photon/(GeV/c) at 37 GeV/c. The calibration constants are therefore 179 photons/(ADC count) for EC31 (*i.e.,* 1790 photons per count of the EC31/10 ADC) and 6045 photons/(ADC count) for EC37. Systematic errors may be of order $\pm 10\%$ due to beam charge toroid calibration, accuracy of foil thickness information, and/or N2MO cross-calibration accuracy.

2.6 Calibration constants used in the last round of n-tuple generation

In the most recent round of n-tuple generation, the N2MO and N3MO ADC readings were converted to total electron counts by multiplying by constants 49 e-/count and 1.8 e-/count, respectively. The corresponding simulation results for these counters were found by integrating the simulated spectrum over the ranges indicated in Table 3, which have widths 0.8 GeV/c and 1.10 GeV/c, respectively. Expressed in the terms of the analysis in this paper, the last round of n-tuple analysis compared the simulated yield of electrons per GeV/c averaged over the given momentum range versus the ADC readings times the constants 61 e-/(GeV/c)/count (for N2MO) and 1.6 e-/(GeV/c)/count (for N3MO). These constants are different from those found here by cross-calibration with ECAL, but

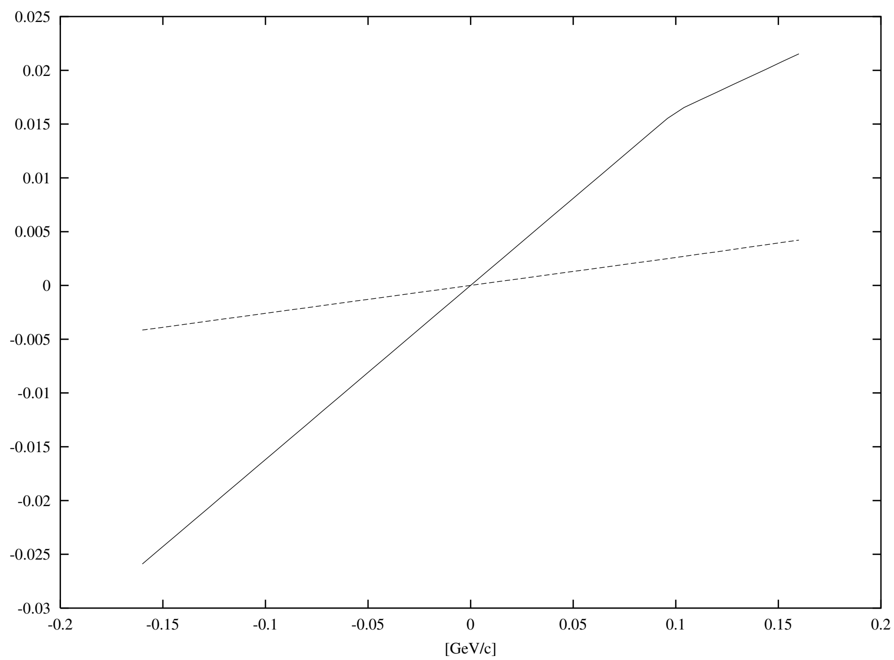

Figure 17: Simulated effect of different central momenta on the accuracy of the calibration of N2MO. Horizontal axis is the shift in GeV/c relative to the nominal central momentum of 12.6 GeV/c. Vertical axis is fractional deviation of the detector yield estimate from its actual value at the nominal central momentum. Solid line is nonlinear Compton data, dashed line is bremsstrahlung.

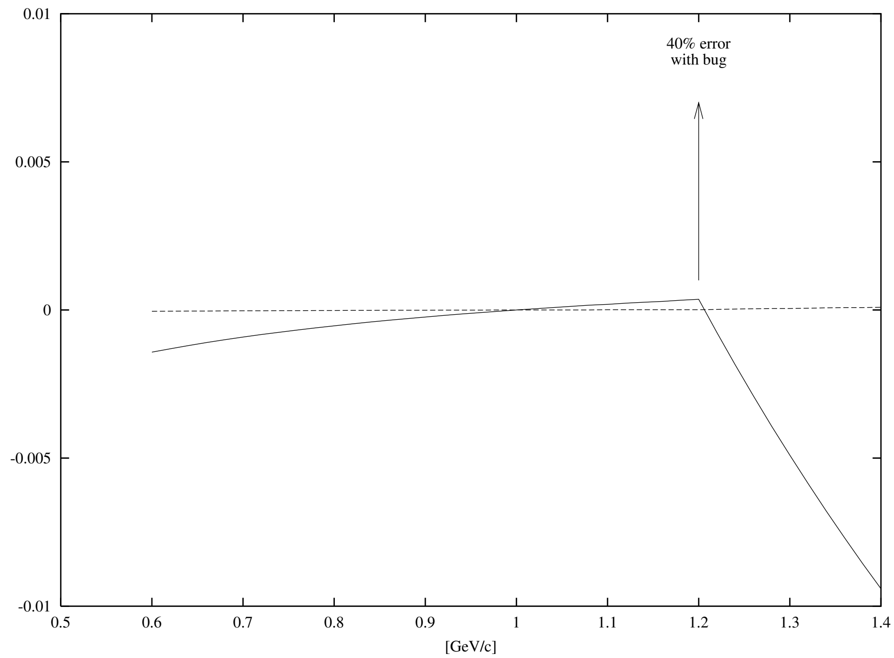

Figure 18: Simulated effect of different central momenta on the accuracy of the calibration of N3MO. (See caption for Fig. 17.) A bug in some early versions of the `sum_bin` function caused an extra bin to be added when the upper end of the acceptance fell exactly on a bin edge.

not by a factor of eight.

The calibration constants for EC31 and EC37 were equivalent to 289 photons/(ADC count) and 8874 photons/(ADC count), respectively.

The "old" calibration constants and those found in the subsections above are summarized in Table 5, and further discussed in the next section.

3 Conclusions

The results of the cross-calibration described above are presented in Table 5 along with the equivalent constants from the original calibration. Table 6 lists the scaling factors used in the original Cherenkov-monitor-based constrained fits [2] and the equivalent scaling accomplished by using the new calibration constants. Although the cross-calibration does not give the same constants as the original calibration, the disagreement is much smaller than that required to explain the factor of eight rescaling done for the constrained fits. According to the cross-calibration, the N2MO and N3MO detectors readings using the old calibration should be scaled by no more than 3.6 and 2.5, respectively.

Furthermore, no adjustment of these newly-obtained calibration constants is required in order to allow good fits of Cherenkov monitors with the simulation. Using the calibration constants of 17 e-/(GeV/c)/count for N2MO and 0.65 e-/(GeV/c)/count for N3MO results in agreement as good as that obtained by large scaling of the original calibration, as detailed in Table 6. Use of these new calibration constants corresponds to scaling the original calibration of N2MO by 3.6 and scaling N3MO by 2.5. The average fitted value of η is $\sqrt{1.8}$ times higher when using the new "adjusted" calibration, a result of the effective scaling with respect to the original differing by a factor of approximately $(1.8)^n$ in each detector. It is interesting that both previous and "new" average η

	calibration constant [e-/(GeV/c)/count]				
detector	original	bremss., Aug. 3	Compton, Aug. 5	bremss., Aug. 8	adjusted for fit
N2MO	61	17 ± 2	—	28 ± 2	15
N3MO	1.6	0.7 ± 0.1	$0.64 \pm .04$	1.4 ± 0.1	0.71

	calibration constant [photons/count]				
detector	original	—	—	bremss., Aug. 7	adjusted for fit
EC31	289			179 ± 20	185
EC37	8874			6045 ± 600	5900

Table 5: Comparison of original calibration with cross-calibration results. Quoted errors include best-guess ranges systematic errors.

	scaling of readouts w.r.t. original				
	NGAMMA	N2MO	N3MO	fit $\langle \chi^2 \rangle$	$\langle \eta_{\rm fit} \rangle$
previous scaling	1.6	8	8	0.9	0.23
new calibration	1.5	4.0	2.3	0.9	0.31
ratio	1.1	2.0	3.5	—	$\sqrt{1.8}$
$0.6 \times (1.8)^n =$	1.1	1.9	3.5		

Table 6: Comparison of effect of the previously-used scaling with the the effect of using the new “adjusted” calibration constants in Table 5. Based on analysis of runs 15296 and 15323. Note that the average value of η calculated from “standard” laser area, pulse length, and measured energy is 0.37.

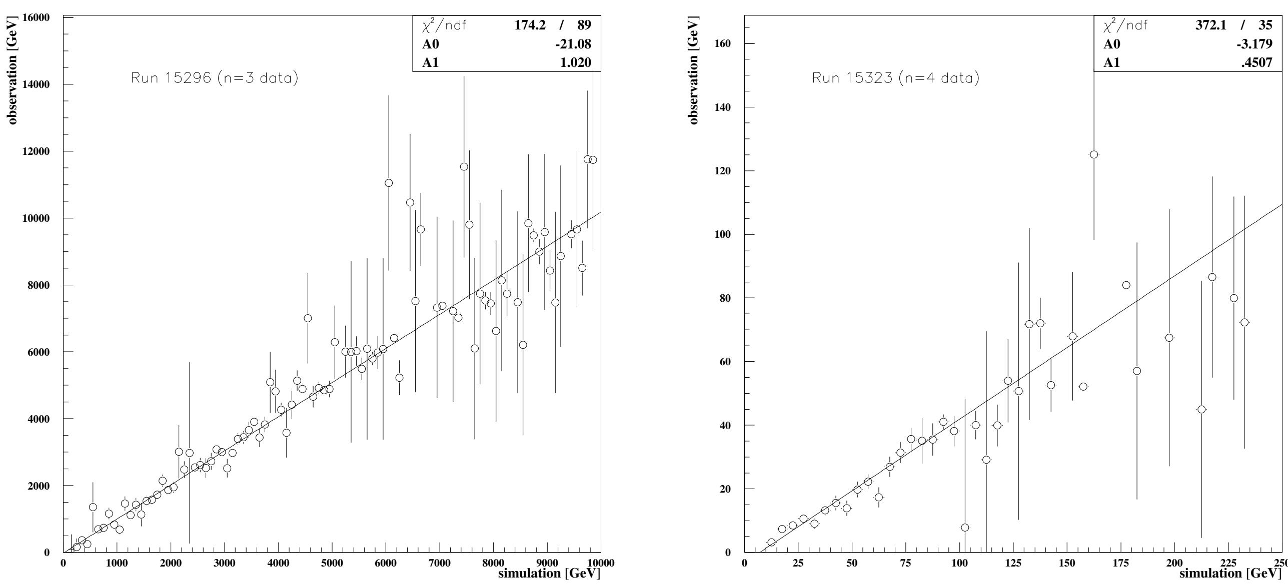

Figure 19: Comparison of experiment with simulation calculated for Cherenkov-monitor-derived η, with new calibration, for two sample runs: 15296 on left, and 15323 on right.

values are less than that calculated from the "standard" laser area, pulse length, and measured energy.

To demonstrate the internal consistency of the new calibration and associated η fits, in Fig. 19 the reconstructed signal (Horton-Smith method) in the top row of ECAL is plotted versus the simulation prediction for runs 15296 and 15323, using all data with only a single cut: $0 < \chi^2_{\eta\text{-fit}} < 10$. Agreement should be almost guaranteed for run 15296, where ECAL is in the $n = 3$ position: the η and overlap are chosen to reproduce the observed signal in N3MO, which has been cross-calibrated with ECAL. In actuality, the observed signal is the same as predicted, demonstrating internal consistency.

The top half of the top row of the ECAL is above the $n = 4$ edge for run 15323. In this case, the observed signal is about half of the simulation. This would not have been considered a "disagreement" in the past, since our intensity estimates were uncertain by $\pm 30\%$, giving a factor of 2.5 uncertainty in normalized $n = 4$ rate and even greater uncertainty in absolute rate. The new calibration reduces systematic uncertainties to the point where this deviation from theory deserves a closer look.

Curiously, the laser intensities from constrained fits with the previous scaled calibration were also about a factor of two lower than the new estimates, which would precisely match the relative rates of the ECAL observations in the two orders, though not the absolute rates.

Shmakov [4] has previously compared the observed ECAL data to spectra simulated for laser laser intensities obtained from the Cherenkov-monitor η fits using the previous scaling. He has found the observation and simulation to be in good agreement, even for cases when the ECAL is directly behind N3MO. Naively, one might not expect this given the new calibration data. If the estimated electron yield from the unscaled N3MO is only a factor of 2.3 too high, and an η is chosen that gives a simulated N3MO reading lower than the actual N3MO reading by a factor of 8, one would expect the simulated ECAL reading of rows in the $n = 3$ region to be lower than observation by about factor of 3.5. This would follow directly from the cross-calibration of N3MO with ECAL using actual $n = 3$ non-linear Compton data. However, since Shmakov compares ECAL data normalized by *unscaled* number of forward photons (using the old calibration) to simulated ECAL data normalized by the simulated number of photons, the expected disagreement between simulation and theory is only $3.5/1.5 \simeq 2$. This is still larger than seen in his analysis. It is just possible that there may have been a compensating factor of two error in the calculation of the simulated N2MO and N3MO signals, or there may be some other subtlety of the analysis that is not obvious upon naive consideration. As mentioned above, any effect bringing the $n = 3$ yield into agreement would also result in excellent agreement for the $n = 4$ agreement due to the lower η estimates in the "scaled" analysis.

In conclusion, the good news is that the cross-calibration apparently eliminates the need for *ad hoc* scaling factors and therefore reduces systematic uncertainties, so that previously-uninteresting inconsistencies between data and theory now become potentially interesting. Additionally, the increased confidence these cross-calibration results provide for the Cherenkov monitors and associated η information is extremely welcome in light of the CCD data, which shows an unexpected relationship between the $\eta_{\text{CCD-fit}}$ and $\eta_{\text{Chernkov-fit}}$. These issues will be addressed in a later paper.

Acknowledgments

The author wishes to thank R. Clive Field and T. Koffas for much helpful dialog and useful information. This work could not have been done without their help, nor would it have been possible without the support of DOE contract DE-AC03-76SF-00515.

References

[1] R.C. Field, "Monitor calibration", in *Proceedings of the [Informal] E-144 Collaboration Meeting, SLAC, January, 1997*, E-144 internal pub., p. 29 (1997).

[2] T. Koffas, private communication (1998).

[3] G. Horton-Smith, "Chi-squared of March '95 data", in *Proceedings of the [Informal] E-144 Collaboration Meeting, SLAC, September 9, 1996*, E-144 internal pub., p. 68 (1996).

[4] K. Shmakov, Ph.D. thesis, U. Tennessee (1997).